Environmental Science and Ecotechnology 21 (2024) 100422

Contents lists available at ScienceDirect

Environmental Science and Ecotechnology

journal homepage: www.journals.elsevier.com/environmental-science-and-ecotechnology/

Original Research

# PAHs removal by soil washing with thiacalix[4]arene tetrasulfonate

Le-Yao Xing [a], Guan-Han Meng [a], Ji-Xian Yang [a, *], Ming-Han Xu [a], Yi-Ming Xu [a], Hai-Xiao Xie [c], Ai-Jie Wang [b], Yi-Lu Sun [b, **]

[a] State Key Laboratory of Urban Water Resource and Environment, School of Environment, Harbin Institute of Technology, Harbin, 150090, China
[b] Key Laboratory of Environmental Biotechnology, Research Center for Eco-Environmental Sciences, Chinese Academy of Sciences, Beijing, 100085, China
[c] Hangzhou Yanqu Information Technology Co., Ltd. Y2, Hangzhou, 310003, China

ARTICLE INFO

*Article history:*
Received 15 August 2023
Received in revised form
15 April 2024
Accepted 15 April 2024

*Keywords:*
Calixarenes
Soil-washing
Host-guest interaction
PAHs

ABSTRACT

Remediating soil contaminated with polycyclic aromatic hydrocarbons (PAHs) presents a significant environmental challenge due to their toxic and carcinogenic properties. Traditional PAHs remediation methods—chemical, thermal, and bioremediation—along with conventional soil-washing agents like surfactants and cyclodextrins face challenges of cost, ecological harm, and inefficiency. Here we show an effective and environmentally friendly calixarene derivative for PAHs removal through soil washing. Thiacalix[4]arene tetrasulfonate (TCAS) has a unique molecular structure of a sulfonate group and a sulfur atom, which enhances its solubility and facilitates selective binding with PAHs. It forms host-guest complexes with PAHs through π-π stacking, OH-π interactions, hydrogen bonding, van der Waals forces, and electrostatic interactions. These interactions enable partial encapsulation of PAH molecules, aiding their desorption from the soil matrix. Our results show that a 0.7% solution of TCAS can extract approximately 50% of PAHs from contaminated soil while preserving soil nutrients and minimizing adverse environmental effects. This research unveils the pioneering application of TCAS in removing PAHs from contaminated soil, marking a transformative advancement in resource-efficient and sustainable soil remediation strategies.



## 1. Introduction

Polycyclic aromatic hydrocarbons (PAHs), specifically those in soil, have been recognized as significant hazards to public health and the environment [1] because of their toxicity, mutagenicity, carcinogenicity, and potential to cause premature mortality, persistent asthma, and respiratory events in children [2]. Soil may represent a constant source of PAHs, leading to long-term environmental damage. Unfortunately, PAHs-contaminated soil is prevalent worldwide, even in polar regions [3,4]. The high organic carbon/water partition coefficient of PAHs makes soil organic matter (SOM) a key factor in PAH adsorption in soil [5,6]. Moreover, tightly bound PAHs present low bioaccessibility, which impedes natural biodegradation-based soil attenuation. Thus, eliminating PAHs from soil and increasing their bioavailability are important tasks.

Most methods used to remediate soils polluted with PAHs have significant drawbacks, including high costs based on oxidants and thermal treatments and the potential to deteriorate soil fertility [7,8]. Other methods, such as phytoremediation and microbial degradation, can be time-consuming, decrease soil nutrients, and produce hazardous degradation products [9,10]. Additionally, using pumps and treatments can limit the mass transfer of the extracting agents [11]. However, soil washing, which involves using washing agents to enhance PAHs solubility and bioavailability and promote PAHs desorption from the SOM, can overcome these limitations.

Surfactants and cyclodextrins are the most widely employed and researched soil-washing agents for PAHs cleanup [12]. However, surfactants may require high concentrations as they can become adsorbed to the soil and are not readily degraded; therefore, they may alter the soil's hydraulic conductivity and cause long-term harm to the ecosystem [13]. Due to these drawbacks, biosurfactants and cyclodextrins have received significant attention because their biocompatibility may aid in biodegradation of PAHs. We propose that an ideal soil-washing agent should (1) not be

* Corresponding author.
** Corresponding author.
*E-mail addresses:* yangxj@hit.edu.cn (J.-X. Yang), ylsun@rcees.ac.cn (Y.-L. Sun).

https://doi.org/10.1016/j.ese.2024.100422

adsorbed by soil or soil organic matter; (2) maintain the soil's characteristics, fertility, and function; and (3) preserve soil microbiological activity. Calixarenes (CAs) meet these requirements [14,15].

Unlike their predecessors, crown ethers (first generation), and cyclodextrins (second generation), CAs have recently attracted substantial interest. This is due to their selective binding properties to hydrophobic aromatic cavities containing small organic molecules, their efficient functionalized upper and lower rims, and their biocompatibility with negligible toxicity [16]. Prior research on CAs has not explored their potential as soil-washing agents or host-guest interactions in organic pollutants remediation. Therefore, our study sheds light on a novel application of CAs, offering valuable insights into their effectiveness in removing organic contaminants.

CAs are a class of cyclic oligomers with distinct structures that can be readily synthesized by reacting phenolic substrates with aldehydes under acidic conditions. By replacing the $CH_2$ linkers of CAs with four S bridges, thiacalixarene (TCA) is endowed with numerous novel properties, such as greater flexibility, which indicates its potential to remove PAHs of various sizes. Moreover, it has transition metal binding ability owing to the S bridges, lone pairs of electrons, and empty 3d orbitals. TCA can remove PAHs and heavy metals concurrently, a property attributed to the multifunctionality of thiacalixarene and its interactions with organic compounds and metals [17,18] by presenting a strong binding capability through electrostatic contact owing to the resonance-like interaction of the unoccupied 3d orbital of sulfide linkages with the orbitals of nearby aromatic rings, which delocalizes negative charges [19,20]. Despite its extraordinary capacity as a receptor, TCA has limited solubility, preventing it from being an additive in water [21]. TCAS, a sulfonated form of TCA, is highly soluble in water and does not compromise cell viability [22]. Although TCA is an excellent receptor, its poor solubility in water has hindered its application as an aqueous additive. Our findings indicate that TCAS presents a valuable alternative due to its water solubility and non-toxic profile, enhancing the solubility of PAHs and heavy metals without detriment to soil ecosystems. We believe our investigation is pioneering in applying CAs and their derivatives to remove organic pollutants via host-guest interactions.

This study examines the potential of TCAS to remove three types of PAHs: naphthalene (Nap), fluoranthene (Flua), and pyrene (Pyr). Our primary focus was on how TCAS interacts with Nap due to the straightforward interaction, which can then be applied to Flua and Pyr [ [23] [24]]. In addition, we evaluated the impact of TCAS on soil ecosystem functions and observed its natural biodegradation properties. This study aims to introduce the CAs family as a new eco-friendly soil-washing agent and explore the possible environmental applications of TCAS.

## 2. Materials and methods

### 2.1. Material

We used naphthalene, fluoranthene, and pyrene for soil spiking and to represent the PAH removal efficiency. These chemicals were purchased from Sigma-Aldrich Co. and had a purity of at least 98%. We selected naphthalene with a purity of at least 99.5% to investigate the interaction mechanism, binding stoichiometry, and constants. The organic solvents included methanol, acetone, dichloromethane (DCM), and dimethyl sulfoxide (DMSO), and they were all high-performance liquid chromatography (HPLC) grade with a purity of at least 99.9%. We prepared a solution with a concentration of 100 mg $L^{-1}$ for naphthalene (Nap), fluoranthene (Flua), and pyrene (Pry) by weighing out 100 mg of each PAH and dissolving them in a specific volume of acetone in a volumetric flask. The solution was shaken for one day at room temperature to obtain a homogeneous mixture.

At the building site of the National Engineering Laboratory of Sludge Safe Disposal and Resource Utilization Technology, clean soil was collected to a depth of 50 cm (Harbin Institute of Technology, No. 73 Huanghe Road, Harbin, China). The soil samples obtained were denoted by the familiar nomenclature 'Sandy Clay Loam', aligning with the parameters delineated by the united states department of agriculture (USDA) classification system, thus ascribing the classification of 'Fine Sandy Clay Loam' to this specific soil type. The clean soil was air-dried, homogenized by handshaking, and then pressed through a 0.50-mm screen to eliminate undesirable particles, such as roots and stones. The PAHs solution was added to 1 kg of sieved soil in a plastic container with 120 cm in diameter and 15 cm in height and mixed well with a spatula for 3 min before being vigorously shaken by hand for 3 min every hour until the acetone evaporated. The soil was placed in a brown jar (diameter: 10.16 cm; height: 15.23 cm) with a wide opening and sealed with a Teflon-lined lid. The sealed soil was then aged for one year in the dark before use.

TCA was first synthesized by Kumagai et al. using a one-step method [25]. In this method, a mixture of p-tert-butylphenol, elemental sulfur (S8), and NaOH was heated under nitrogen in tetraethylene glycol dimethyl ether (Fig. 1). TCA was then sulfonated using a direct sulfonation procedure initially proposed by Iki et al. [26]. By controlling the amount of oxidizing agent, TCA afforded a sulfonyl analog (Fig. 2).

### 2.2. Soil characterization

Before conducting batch experiments to assess soil washing efficiency, the soil was characterized to determine its properties and composition. Soil pH was measured at a soil-to-liquid ratio of 1:2.5 (weight/volume) using a pH meter (PHSJ-3F, Leici, Shanghai). The relative proportions of clay, sand, and silt were calculated using the hydrometer method described by Miller et al. [27]. The cation exchange capacity (CEC) of the chosen soil was measured using the Environmental Protection Agency (EPA) method 9081 [28]. The total organic matter of the soil was measured by the method described by Ramos et al. [29]. The total amounts of nitrogen, phosphorus, and potassium were determined using the technique described by Lin et al. [30]. The isolation of soil organic matter fractions, encompassing humic acids (HAs), humins (HNs), and fulvic acid (FAs), primarily adhered to the protocols detailed by Ukalska-Jaruga et al. [31]. Subsequently, the distinct components of soil organic matter were quantified utilizing the methodology elucidated by Jez et al. [32].

The impact of TCAS on soil quality components, including nitrogen hydrates (NHs), humic acids (HAs), humic fractions (HFs), total nitrogen (TN), and total potassium (TK), is defined by washing 100 mg of clean soil with 1 L of 0.3% TCAS solution and 3.0% TCAS solution separately.

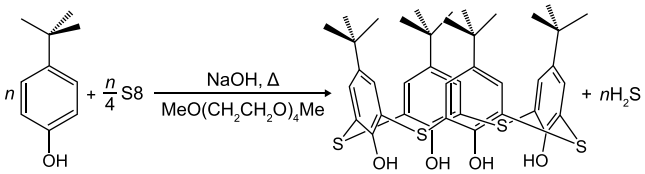


**Fig. 1.** Synthesis scheme of TCA.

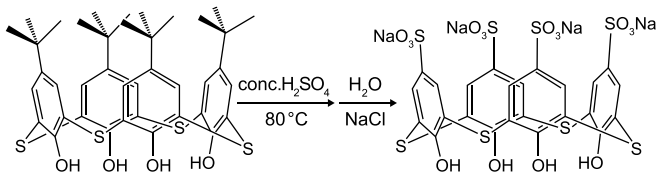


**Fig. 2.** Synthesis scheme of TCAS.

### 2.3. Batch experiments

Triplicate batch tests were conducted to examine the desorption kinetics and effects of pH, soil-to-liquid ratio, and TCAS concentration on soil washing efficiency. Before each test, 0.5 g $L^{-1}$ $HgCl_2$ was added to inhibit the biodegradation of PAHs and TCAS. Each sample was allowed to settle and centrifuged to generate a moderately dry soil sample for PAHs extraction. HPLC analyses were performed following each experiment.

For the kinetic investigations, 5 g of spiked soil and 10 mL of TCAS (0.3 mM) were added to 100 mL Erlenmeyer flasks. The kinetic study was conducted at pH 7.0, a soil-to-liquid ratio of 10:1, a TCAS concentration of 0.7%, and a temperature of 25 °C. The flasks were shaken for 0–8 h at 200 rpm in an incubator shaker.

The soil-to-liquid ratio was studied at a constant pH of 7.0, a TCAS concentration of 0.7%, and a temperature of 25 °C. The ratios adjusted ranged from 1:5 to 1:20, and the samples were shaken for 12 h at 200 rpm.

TCAS solutions (0.1–0.9% w/v) were prepared for the concentration study. This study was performed at a consistent pH of 7.0 and a soil-to-liquid ratio of 10:1. The samples were also shaken for 12 h at 200 rpm and 25 °C.

For investigating the impact of pH on the removal efficiency of TCAS, each assay commenced with a calibration of the pH meter against citrate, phosphate, and borate buffer solutions at pH 4.0, 7.0, and 10.0, respectively, to ensure accurate pH control in the soil washing solution. The pH was initially set using HCl or NaOH, then strategically adding these buffers to maintain constant pH levels, facilitating a targeted investigation into the pH's influence on soil washing efficiency. The experiments were conducted at 25 °C, a TCAS concentration of 0.7%, and a shaking duration of 12 h at 200 rpm.

### 2.4. PAHs analysis

The PAHs in the spiked were first extracted using the US EPA 1996 technique [33], followed by quantitative analysis using HPLC. Briefly, 5 g of soil was pulverized with 10 g of sodium sulfate, followed by Soxhlet extraction with 300 mL of acetone/hexane (1:1) (v/v) for six cycles per hour for 16 h. The solvent was then reduced to approximately 1.5 mL using a rotary evaporator and nitrogen blower. After extraction, the solvent was removed by adding 50 mL acetonitrile, followed by the same procedure until the liquid reached 1 mL. They were then passed through an $Al_2O_3$-filled Pasteur pipette for cleaning. The cleaned solvent was transferred to an HPLC chromatography vial and subjected to gradient HPLC on an Agilent 1200 Series system with an Agilent ZORBAX Rapid Resolution High-Definition Eclipse-threaded polynuclear aromatic hydrocarbon (PAH) (2.1 × 100 mm, 1.8 μm) columns. The HPLC parameters included 0.9 min of isocratic elution by acetonitrile/water (4:6) (v/v), followed by 14.5 min of gradient elution to 100% acetonitrile at a flow rate of 0.42 mL $min^{-1}$ at 30 °C. The UV detector was set at 220 and 230 nm. The final PAHs concentrations and soil characteristics are listed in Table 1.

The quantification of PAHs liberated into the TCAS soil-washing solution was performed using a rigorous liquid-liquid extraction method. In brief, a 5 mL aliquot of the washing solution was procured after the soil-washing step. This aliquot was centrifuged at 7000 rpm for 10 min and then passed through a 0.45 μm filter to remove residual soil particulates. The filtrate was then diluted tenfold with deionized water and introduced into a 500 mL separatory funnel. Then, 20 mL of dichloromethane (DCM) was added. The mixture was vigorously shaken for 2 min and then left to settle for 5 min to separate the layers. The PAH-containing organic layer was collected, and the extraction process was repeated twice. The combined organic extracts were dried over anhydrous sodium sulfate with the volume subsequently to 1 mL using a rotary evaporator followed by a nitrogen stream. The concentrated extract was then transferred into vials suitable for high-performance liquid chromatography (HPLC) analysis. The removal efficiency was calculated as follows:

$$RE = 1 - \frac{WS_{PAHs} - WSol_{PAHs}}{IS_{PAHs}} \times 100\% \quad (1)$$

where RE stands for Removal Efficiency (%); $WS_{PAHs}$ refers to the residual concentration of PAHs in the soil post-washing; $WSol_{PAHs}$ indicates the PAHs mobilized from the soil into the washing solution; $IS_{PAHs}$ denotes the baseline concentration of PAHs in the soil before applying any washing procedures.

### 2.5. TCAS adsorption experiment

The adsorption experiments were performed to quantify the uptake of a novel soil washing agent, TCA, on two soil types: pristine and PAHs-contaminated. The procedure maintained a constant temperature of 25 °C and a pH of 7.0. A soil-to-liquid ratio of 1:10 was employed, with 5 g of soil used for each trial.

TCAS solutions were prepared at concentrations ranging from 0.0 to 1.0% (w/v) for adsorption. Each soil sample was contacted with the TCAS solution, and the mixtures were incubated in an orbital shaker set at 100 revolutions per minute for 12 h, which was determined to be the equilibrium time in preliminary studies. Post incubation, the concentration of the remaining TCAS was estimated based on the decrease in TCAS concentration during soil cleaning. The TCAS concentration was determined by adding an excessive quantity of Nap to 2 mL supernatant, shaking the solution at 30 °C for 48 h to achieve equilibrium, centrifuging it at 5000 rpm for 10 min, and filtering out any Nap precipitation. A 1 mL solution was diluted with 9 mL (5:5) methanol/water to fully extract Nap from the TCAS-Nap complex. Based on the results of the spectrophotometric measurements, the concentration of Nap determined via HPLC was approximately equivalent to that of TCAS.

### 2.6. Characterization of TCAS-Nap complex

As the mechanisms underlying the ability of TCAS to remediate pollutants have never been exhaustively studied, this research focuses primarily on the binding methods of Nap-TCAS to avoid potential misunderstandings. Based on the findings of the spectrophotometric experiments, the TCAS-Nap complex with a 1:1 M ratio was produced in DMSO. After shaking for 24 h, the solution was freeze-dried and evaporated using a rotary evaporator, and then the powder was collected for further characterization.

PXRD was performed on TCAS, Nap, and TCAS-Nap using Cu K radiation and a Rigaku Ultima IV diffractometer. The fourier-transform infrared (FT-IR) spectra were recorded on a Thermo Scientific Nicolet iS20 using the KBr disc technique with a resolution of 4 $cm^{-1}$. The 1H NMR spectra were acquired using a BRUKER AVANCE 400 NMR spectrometer with 4 mg of the powder

**Table 1**
Physicochemical property, texture, and PAHs concentration of the spiked soil.

| Soil properties | | Value |
|---|---|---|
| Physicochemical properties | pH | 6.24 ± 0.13 |
| | CEC (cmol $kg^{-1}$) | 17.93 ± 0.87 |
| | TOC (g $kg^{-1}$) | 40.52 ± 0.92 |
| | TN (g $kg^{-1}$) | 1.92 ± 0.04 |
| | TP (g $kg^{-1}$) | 1.06 ± 0.02 |
| | TK (g $kg^{-1}$) | 17.89 ± 1.62 |
| | NHs (mg $kg^{-1}$) | 2.91 ± 0.25 |
| | HAs (mg $kg^{-1}$) | 8.13 ± 0.78 |
| | HFs (mg $kg^{-1}$) | 2.51 ± 0.24 |
| | HNs (mg $kg^{-1}$) | 15.31 ± 1.78 |
| Texture | Clay (%) | 35.62 |
| | Silt (%) | 26.58 |
| | Sand (%) | 36.80 |
| PAH concentration after spike | Nap (mg $kg^{-1}$) | 90.25 ± 3.98 |
| | Flua (mg $kg^{-1}$) | 91.69 ± 3.07 |
| | Pry (mg $kg^{-1}$) | 92.53 ± 2.81 |

Abbreviations: CEC: Cation exchange capacity; TOC: Total organic carbon; TN: Total nitrogen; TP: Total phosphorus; TK: Total potassium; NHs: Nitrogen hydrates HAs: Humic acids; HNs: Humins; FAs: Fulvic acid; Nap: Naphthalene; Flua: Fluoranthene; Pry: Pyrene.

completely dissolved in DMSO $d_6$. The morphology was examined using a Zeiss Sigma 300 microscope.

Ultraviolet (UV) spectrophotometric analysis was performed using a SHIMADZU UV-3600 dual-beam UV−visible spectrophotometer (Kyoto, Japan). The fluorescence spectra were obtained using a Hitachi f7000 fluorescence spectrophotometer. The excitation wavelength was 280 nm, and the excitation and emission bandwidths were 2 nm.

### 2.7. Computational strategy

The interaction between TCAS and Nap was analyzed using density functional theory and Gaussian 09 [34], a computational chemistry tool for electronic structure modeling licensed from Gaussian, Inc. The M06-2X [35] hybrid exchange-correlation functional with 6-31G (d,p) basis sets were used to determine and calculate the electronic energy. The thermodynamic energy of each species consisted of the computed electronic energy (Emol), thermal correction to the Gibbs free energy (ΔGc), and solvation energy of the copper complex (ΔGsol). The solvation energy at the M05-2X [36]/6-31G* [37] level was determined using the Solvation Model based on Density (SMD) within the framework of computational chemistry. An independent gradient model based on the independent gradient model of Hirshfeld (IGMH) [38] analysis was performed, and it revealed a weak interaction between TCAS and NAP. The IGMH spatial 3D output was rendered using VMD software. The Multiwfn and Gnuplot packages processed color-filled maps for the specified cross-section. An electrostatic potential map was created using the cubegen tool in the GaussView 5.0 program and processed using the Multiwfn package [39]. Visualization work was performed using the VMD package. Time-dependent density functional theory (TDDFT) was used to compute the electronic spectrum of TCAS-Nap. Twenty excitation states were computed by appropriately truncating the excitation energy (2 eV for TCAS-Nap) to plot the theoretical spectrum.

### 2.8. Soil respiration rate and enzyme activity measurement

We conducted soil respiration and enzyme assays under controlled laboratory conditions. Fresh soil (10 g) was placed in a 1 L amber glass jar and incubated at 15 °C with 85% relative humidity for 24 h in a dark environmental chamber. We adjusted the soil moisture content to approximately 65% of its field capacity by adding 6.5 mL of a TCAS solution prepared at concentrations of 0.3% and 3.0%.

The rate of $CO_2$ evolution in TCAS-washed soil was assessed using the method described by Angers et al. [40]. The amount of $CO_2$ generated was estimated by back-titrating NaOH with 0.5 M HCl in 5 mL of 1.5 M $BaCl_2$.

To investigate the effect of TCAS on soil quality, we analyzed changes in the activity of β-glucosidase (βGA) soil enzymes: Clean soil washed with 0.3% TCAS and 3.0% TCAS was incubated at 20 °C and 80% of its water-holding capacity for one week. The enzyme activity of βGA was measured as previously described by Tabatabai et al. [41].

### 2.9. Statistical analysis

In this study, soil samples were washed in three independent experiments to assess changes in nutrient concentrations. Results are reported as mean ± standard deviation, and we performed the analysis using SPSS 16.0 software. Statistical significance between the treated and untreated soil samples was determined using a one-way ANOVA, followed by a post hoc Tukey's HSD test. Significant distinctions are indicated by varying letters.

## 3. Results and discussion

### 3.1. Experimental analysis of interaction mechanism

FT-IR, PXRD, and 1H NMR spectroscopy provided information on the binding mechanism of TCAS and Nap.

The FT-IR spectra underwent a considerable transformation after fixation with TCAS and Nap (Fig. 3a). A broad and strong band for TCAS, which was ascribed to the typical “polymeric” OH stretching at 3350 $cm^{-1}$, shifted up to 3386 $cm^{-1}$ in the presence of Nap; nevertheless, a tiny and sharp peak at 3472 $cm^{-1}$ indicated the presence of the hydroxyl group, as shown by the redshift of up to 10 $cm^{-1}$ [42,43]. The strengths of both peaks decreased once the complex was produced. A “pit” covering the whole region from 3697 to 3100 $cm^{-1}$ was developed when the separation between the two peaks decreased. This may be because the TCAS-Nap complex increased the density of accessible states owing to its poor symmetry and increased number of normal modes [44]. Moreover, the red shift of the OH stretch may be a direct result of intramolecular OH interactions between the OH group and segment of the Nap π-electron plane embedded near the lower rim of the cavity, and such a weak interaction may also have contributed to the decrease in the intensity of the OH stretch [45].

The formation of an inclusion complex resulted in the disappearance of the out-of-plane CH vibrations of aromatic rings at approximately 800 $cm^{-1}$ for Nap, indicating a constraint on the out-of-plane CH vibration of aromatic rings [46]. Furthermore, a blue shift of approximately 4 $cm^{-1}$ was observed for the C═C stretching of aromatic cavities at 1662 $cm^{-1}$ and the phenolic units at 1123 $cm^{-1}$ of TCAS. The distortion of the TCAS cavity may have been caused by electrostatic withdrawal induced by the electrophilic outer side of the Nap molecule, which is also valid for structural optimization.

Furthermore, powder X-ray diffraction (PXRD) was used to determine the probable solid-state complex formation process. The XRD patterns of TCAS, Nap, and their 1:1 M ratio-powered systems are shown in Fig. 3b. The uniqueness of the XRD pattern displayed by TCAS and its Nap complex was readily apparent. Compared with the XRD pattern of TCAS, as observed in zones 1, 2, and 3, the Nap-guest complex had broader and weaker peaks, and the background noise also increased. These discrepancies suggest that the addition

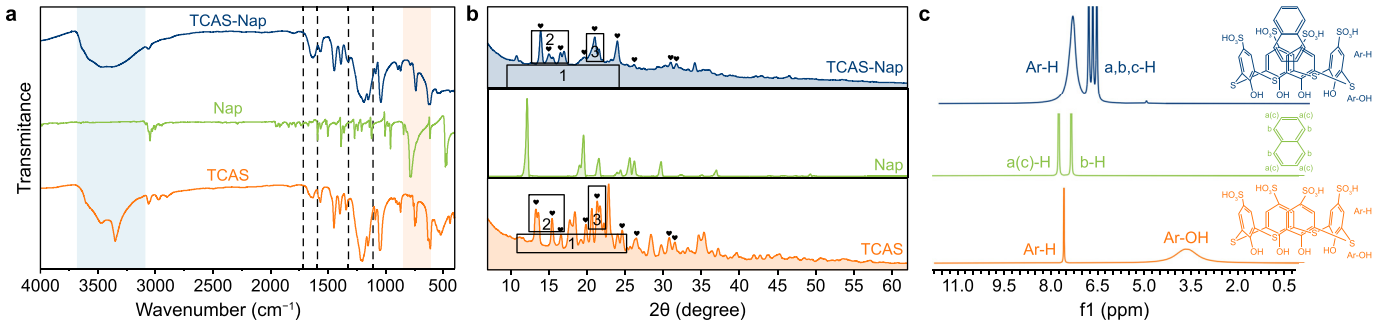


**Fig. 3.** The FT-IR (**a**), XRD (**b**), and NMR (**c**) analysis of TCAS, Nap, and TCAS-Nap.

of Nap may impair the crystallinity of the structure, which is consistent with the discovery that the interaction between the guest and host can expand and diminish the XRD peaks [47]. Despite the formation of the TCAS-Nap complex, the characteristic peaks shared by TCAS and the newly created complex and slight changes in distinct peaks were surprising (Fig. 3b, black hearts). This resemblance may be attributable to the fact that the TCAS cavity (1.78 Å) was greater than the size of Nap (1.37 Å), which interfered with the TCAS structure; hence, the crystalline structural arrangement varied slightly [48].

The overlay of the NMR spectra for TCAS, Nap, and their 1:1 ratio complex in DMSO (Fig. 3c), serves to illustrate the likely binding mode between Nap and TCAS, evidenced by shifts in chemical shift values (Δδ). TCAS assigns Ar−H and Ar-OH to aromatic protons and hydroxyl and uses a,b,c-H to protons in the upper, middle, and lower Nap molecular positions. The NMR result should be interpreted in light of the particularly inconvenient coincidence that the Ar−H signal, which peaked at 7.81 ppm, was close to the protons of Nap, which peaked at 7.91 and 7.52 ppm. As a result, some Nap proton signals may be obscured by the TCAS signal. Due to the π-π interaction between the aromatic wall of TCAS and Nap, the Nap protons likely experience a shield effect after complexation, and their chemical shift values will be placed in the upfield region [49−51]. Although a sizeable upfield shift was found in the Nap protons, the formation of a new peak was highly unexpected because such a phenomenon has rarely been reported in prior research [52−55]. Despite the novelty of the newly created peak, there may be a rationale for this observation. Nap is inserted partially into the anisotropic aromatic TCAS cavity, and the π-electron plane of Nap forms an O−H bond with the hydroxyl group located in the lower rim of the TCAS cavity; consequently, the C−H protons of Nap have a more pronounced chemical upshield. These results are complementary to those obtained via FT-IR spectroscopy.

In addition, the incorporation of Nap considerably widened the Ar−H peaks. The expanded peak of the aromatic protons of TCAS may be attributed to the local field experience of TCAS aromatic nuclei caused by the complexation of Nap as the molecule tumbles, inducing relaxation [56].

### 3.2. Structure and morphology of TCAS and its host-guest complex

The TCAS-Nap complex was obtained after Nap complexation. SEM was then used to study the structure and morphology of the two types of particles (Fig. 4). In the presence of Nap, the particle size decreased from approximately 0.2−0.8 to 0.1−0.5 μm, and the surface became rougher than that of the unmodified TCAS. The crystalline structure of the complex underwent considerable modification. The TCAS particles comprised 3−15 irregular, mostly prismatic thin plates with poor and uneven crystalline morphologies. The XRD spectra confirmed that the plate-shaped particles acquired a crystalline morphology following their appearance. The Nap-TCAS complex particles resembled a TCAS particle rotated by 90°, although they were smaller and had fewer defined boundaries. The structural resemblance between the host and host-guest complexes has been infrequently observed in previous studies [53,55,57,58].

### 3.3. Binding stoichiometry and binding constant by spectral titration

As shown in Fig. 5a, the UV−vis spectra of Nap, TCAS, and their mixtures at various molar ratios were compared to determine the binding stoichiometry of the TCAS and Nap complex. The TCAS and Nap concentrations were mixed up at different concentrations, whereas the total concentration of [TCAS]+[Nap] was kept constant. The molar ratio of Nap was expressed as $R_{Nap}$ $\{R_{Nap} = \frac{[Nap]}{[TCAS]} + [Nap]\}$. TCAS could absorb UV light with maxima at 257.2 and 310.5 nm. However, no adsorption bands were observed in the 300−360 nm range, and weak absorbance bands were observed in the 254−300 nm range without recognizable adsorption maxima. As the Nap fraction increased, TCAS adsorption bands gradually transformed into Nap adsorption bands, and the 1:1 ratio host-guest complex exhibited a fusion of the Nap and TCAS adsorption maximum features. This suggests that TCAS and Nap form host and guest inclusion complexes. The reliable job plot method was used to evaluate the stoichiometry of the inclusion

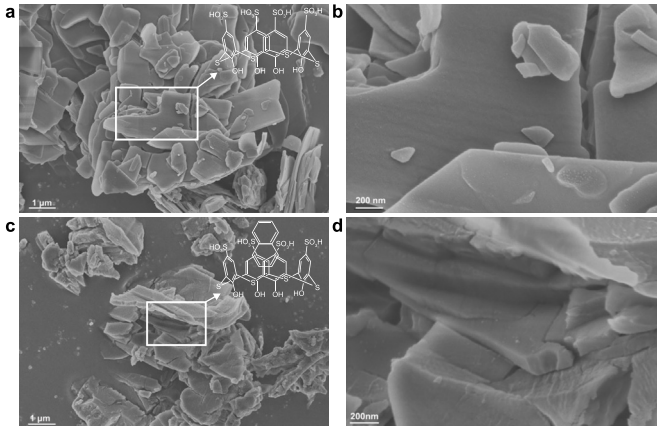


**Fig. 4.** SEM images of TCAS and TCAS-Nap complex. **a**, TCAS microstructure at low magnification; **b**, Zoomed-in detail of TCAS microstructure. **c**, TCAS-Nap complex microstructure at low magnification. **d**, Zoomed-in Detail of TCAS-Naphthalene complex microstructure.

complexes [59]. A solution containing 2 mM Nap and TCAS was prepared, and the combined concentration of the components was maintained at 0.2 mM. Nap solutions with molar fractions ranging from 0 to 1 were then prepared and analyzed. In our analysis, the *x*-coordinate designated as '$R_{Nap}$' corresponds to the molar fraction of Nap, while the term '$\Delta A \times R_{Nap}$' refers to the product of the change in absorbance ($\Delta A$), which is the absorbance differential of Nap in the presence and absence of TCAS and the molar fraction of Nap. For further clarity and reference, the comprehensive titration strategy employed is detailed in Table S1. Similar to many other CAs complexes, the highest point of the job curve was reached at a Nap molar fraction of approximately 0.5, indicating a 1:1 stoichiometry (Fig. 5b). Computational investigations further validated these 1:1 binding characteristics. More developed structures were optimized [60–62].

Fluorescence emission spectra were used to investigate the binding processes. Fig. 5c shows the fluorescence emission spectra of 0.2 mM Nap in the presence of different concentrations of TCAS. As shown in Fig. 5c, the introduction of TCAS reduced the fluorescence intensity of the Nap molecule. Adding TCAS increased the polarity around the Nap molecule, which typically leads to solid quenching owing to hydrogen bonds and electrostatic interactions. To further analyze the data from the fluorescence emission spectra, the Benesi-Hildebrand approach was used, which effectively interprets the binding stoichiometry of the host and guest complexes [63–65]. The job plot indicates that the inclusion behavior adheres to a 1:1 binding pattern. Therefore, the Benesi-Hildebrand equation is as follows:

$$\frac{1}{\varnothing_f^0 - \varnothing_f} = \frac{1}{\varnothing_f - \varnothing_{complex}} - \frac{1}{\left(\varnothing_f - \varnothing_{complex}\right) K[TCAS]} \quad (2)$$

where $\varnothing_f^0$(AFU) and $\varnothing_f$(AFU) represent the emission intensities either exclusive or inclusive of TCAS, respectively, and $\varnothing_{complex}$(AFU) estimates the fluorescence intensities of all Nap molecules in TCAS. The line of best fit is plotted at 1 divided by the denominator of $\varnothing_{complex}$(AFU) versus $\frac{1}{[TCAS]}$($M^{-1}$), as shown in Fig. 5d. The K ($M^{-1}$) value, which is calculated from the slope and intercept of the fitted line, was 4.56 × 103 $M^{-1}$, indicating a strong interaction. Using equation (2), the standard Gibbs energy change ($\Delta G_0$) was −20.9 KJ.

$$\Delta G^0 = -2.303RT \lg K \quad (3)$$

where R is the gas constant (equal to 8.3145 J $mol^{-1}$ $K^{-1}$), T represents the experiment temperature.

### 3.4. Computational study of the interaction mechanism of TCAS and PAHs

The geometric structures of TCAS, Nap, and their complexes were optimized. The TCAS structure with the lowest energy adopted a cone conformer, with the phenolic OH groups on the lower rim linked by sulfide and sulfonate groups on the upper rim, as depicted in Fig. 6a. The distance between $O_1$ and $O_3$ on the lower

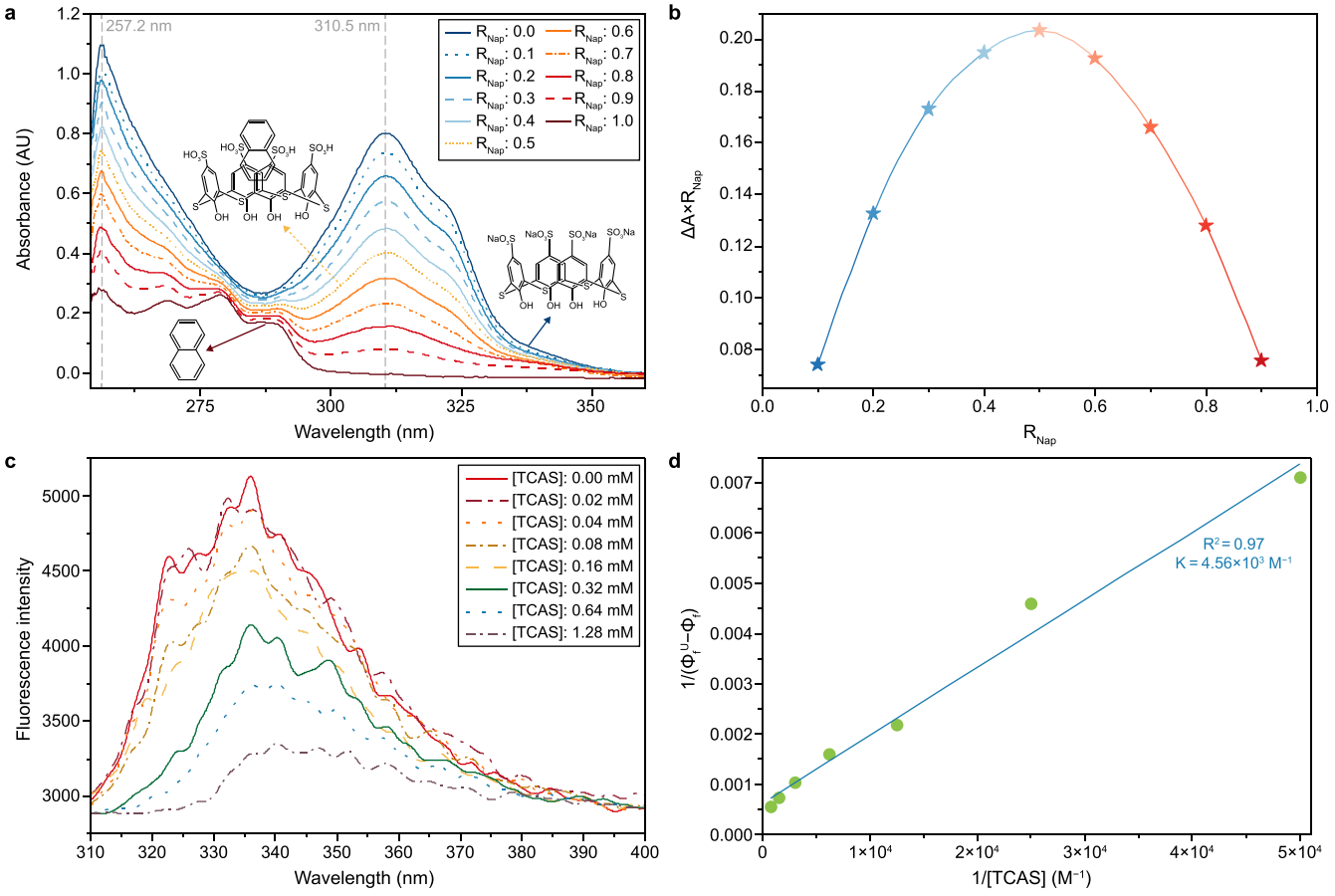


**Fig. 5.** **a**, UV–vis spectra of different mole ratios of TCAS and Nap. **b**, Job's plot for UV–vis titration. **c**, Fluorescence titration of different molar ratios of TCAS and Nap. **d**, Benesi-Hildebrand plot for fluorescence titration.

rim was 3.68 Å. Thus, TCAS can easily accommodate the Nap molecule (1.42 Å) due to their size compatibility, as shown in Fig. 6b. Fig. 6c shows the docking of Nap to TCAS. Our computational findings were consistent with the NMR spectra, in which Nap was partially enclosed in the TCAS cavity from the top of the TCAS cone. The lowest negative binding energy (ΔG) of the most stable TCAS-Nap configuration was −253.6 kcal $mol^{-1}$. The complexation with Nap significantly altered the size of the TCAS cavity. For instance, in the TCAS-Nap complex, the distance between the intramolecular hydrogen bonds on the upper and lower rims produced by the OH and $SO_3^-$ groups, as determined by the lengths of $H_1$−$O_2$ and $S_1$−$S_2$, respectively, was elongated by approximately 0.18 and 0.294 Å, compared to that of the single TCAS. The steric barrier between the flexible TCAS cavity and Nap explains the expansion of the host cavity. Other studies have also reported variations in the cavity diameter [66–68].

To further elucidate the TCAS-binding sites and charge distribution in the TCAS-Nap complex, we measured the electrostatic potential of individual molecules on the van der Waals (vdW) surface. The entire vdW surface had a negative electron potential because of the highly electronegative and electron−withdrawing properties of the $SO_3^-$ group (Fig. 6e–h). The $SO_3^-$ groups of TCAS process the highest negative electrical value (−9.64 to −9.79 eV) of electrostatic potential, mostly located on the O atom of the sulfonate groups. A less electron-negative area formed around the TCAS cone due to the withdrawal of the aryl rings' electron density; a Vmax zone with a value of about −7.17 eV may even be detected. In conclusion, depending on the nucleophilic and electrophilic nature of the guest molecule, an active binding site may be found on either the lower or higher rim of the TACS cavity. Fig. 6f and i show the electrostatic potential distributions of the Nap molecules. A negative adjacent bond forms in the core of the Nap molecule, and the blue areas around it show the positive sections of the molecule that lack electrons. The greatest positive and negative values were 14.33 and −17.16 eV, respectively. The electron-rich sites of the Nap molecule were located at the center of the Vmin sites on the upper rim of TCAS to maximize electron attraction. Despite the strong electron attraction, repulsion will likely occur between the unsaturated negative π regions of the aromatic rings of TCAS and Nap. The flexible TCAS cavity enlarged because the $SO_3^-$ facing the negative sides of the Nap molecule became increasingly unattached and even formed a rhombus. Fig. 6g and j shows that the TCAS-Nap complex was electron-negative after encapsulation. Only 40% of the vdW surfaces had a relatively negative molecular electrostatic potential (MESP) value (7.5 eV), whereas 90% of TCAS had a more negative value. In addition, the $SO_3^-$ group visibly withdrew electrons from Nap. A charge transfer occurred between TCAS and Nap. When interacting with a guest molecule, the negative MESP on the TCAS vdW surface may behave as a hydrogen acceptor. The IGMH analysis could provide a more visual understanding of the host-guest hydrogen bond.

The electron transfer behavior in excitations of the TCAS-Nap complex was analyzed. Fig. 6m shows the topologies of a few molecular orbitals involved in the host-guest electron transitions, and Fig. S1 shows the theoretical absorption spectra. At oscillator strengths of 0.039, 0.414, 0.196, and 0.040, four primary absorption bands at 279.86, 272.66, 266.12, and 258.98 nm were calculated, respectively (Table S2). Because the highest occupied molecular orbital (HOMO) entirely resides on the Nap molecule and the lowest unoccupied molecular orbital (LUMO)+3 is confined over Nap and the TCAS cavity, the band at 279.86 nm results from the interaction between the Nap molecule and the hydrophobic cavity of TCAS. Because the most predominant electron transition from (HOMO+1, HOMO+3) to (LUMO+4, LUMO+2) occurs on the phenolic OH group and part of the Nap molecule that enters the TCAS cavity, this phenomenon indicates hydrogen bonds between TCAS and Nap. The experimental results also confirm the development of hydrogen bonds.

For the assembly configuration, the independent gradient model of Hirshfeld (IGMH) analysis was performed to better understand the interactions between the host and guest (TCAS and Nap) molecules. In particular, the second Hessian eigenvalue ($\lambda_2$) allowed us to discriminate between the distinct forms of interaction. The sign ($\lambda_2$) function, which signifies repulsive or attractive interactions, was mapped onto isosurfaces using different colors to visually define the nature of the interactions. $\lambda_2 < 0$ stands for bonding interactions; $\lambda_2 > 0$ represents nonbonded contact, such as steric repulsion; and $\lambda_2$ slightly below 0 represents vdW interactions [69], and ρ designates the product of electron density. The isosurfaces are colored according to the following sign ($\lambda_2$) color scheme: blue for attractive weak interactions like hydrogen bonds, green for vdW interactions, and red for repulsive interactions like steric and electrostatic repulsion (Fig. 6i). The OH bond (blue area) and electric repulsion (red zone) can also be found in the inner Nap, as predicted by the MESP analysis. Fig. 6k–l shows a green-blue region between the peripheral of Nap and TCAS, which is representative of the π-π interactions. However, as predicted by the MESP analysis, an OH bond (blue area) and electric repulsion (red area) could also be found in the inner Nap. The negative-negative electron repulsion between the inner Nap and TCAS can explain this repulsion.

### 3.5. Removal efficiency of PAHs

The desorption capabilities for Nap, Flua, and Pyr are displayed in Fig. 7, and the sequence of desorption efficiencies observed was as follows: Nap exhibited a higher rate than pyrene Pyr, which in turn was more efficient than Flua. Under controlled conditions, with a soil-to-liquid ratio of 1:10 and at pH 7, applying 0.7% TCAS facilitated the removal of 55.12% of Nap, 47.66% of Flua, and 49.98% of Pyr.

The molecular size is a critical determinant in the efficacy of CAs in host-guest interactions, with a marked preference for TCAS for smaller guest molecules [70]. However, modulation of the TCAS cavity size may offer a route to optimize host-guest interactions [66], potentially mitigating the influence of molecular dimensions on desorption efficiency. In the case of TCAS-Nap, electrostatic forces predominantly facilitate the interaction, with a discernible correlation between removal efficiency and the resonance energy (RE) of the PAHs, a function of their electron count.

A time-course analysis over 480 min indicated that PAH desorption reached an equilibrium within the initial 100 min, beyond which the desorption levels plateaued (Fig. 7a). Notably, a TCAS concentration of 0.7% was identified as optimal for PAH removal. Further increments in TCAS did not proportionally increase desorption rates, possibly due to the saturation of binding sites, leading to a hypothesized 1:1 stoichiometric complex between TCAS and Nap (Fig. 7c). The soil-to-liquid ratio was optimized at 1:10; deviations from this ratio did not enhance the PAHs desorption efficiency, likely attributable to decreased TCAS interaction (Fig. 7b). The desorption efficiency of TCAS for PAHs is significantly influenced by pH levels. In acidic conditions, the sulfonate groups on TCAS are protonated, creating electrostatic repulsion that impedes close interaction with PAHs, thus reducing desorption efficiency. However, as the pH becomes basic, these groups deprotonate, decreasing electrostatic repulsion and enhancing the affinity between TCAS and PAHs. This deprotonation at higher pH values improves interaction through mechanisms such as π-π stacking, which is crucial for desorption [71]. The reduction in repulsion under basic conditions also aids in releasing

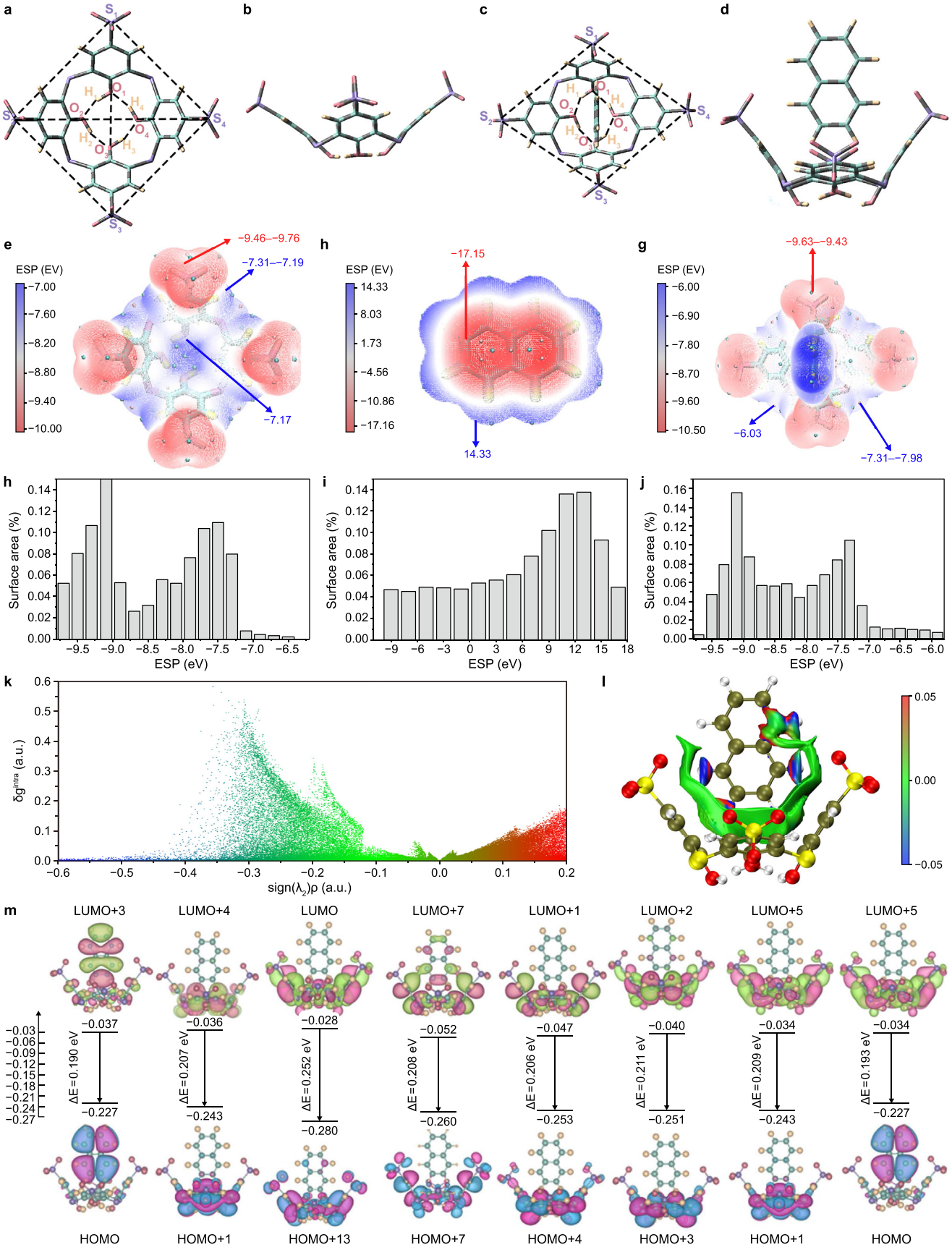


**Fig. 6.** **a**–**b**, Optimized structures of TCAS: the front (**a**) and top (**b**) view. **c**–**d**, Optimized structures of TCAS-Nap: the front (**c**) and top (**d**) view. **e**–**g**, Electrostatic potentials on the van der Waals surface of TCAS (**e**), Nap (**f**), and TCAS-Nap (**g**). **h**–**j**, Distribution analysis of TCAS (**h**), Nap (**i**), and TCAS-Nap (**j**) highlighting electrostatic potential regions. **k**–**l**, IGHM analysis of TCAS-Nap complex: RGD scatter plots (**k**) and isosurface density maps (**l**). **m**, Molecular orbital topologies of TCAS-Nap: HOMO to LUMO progression.

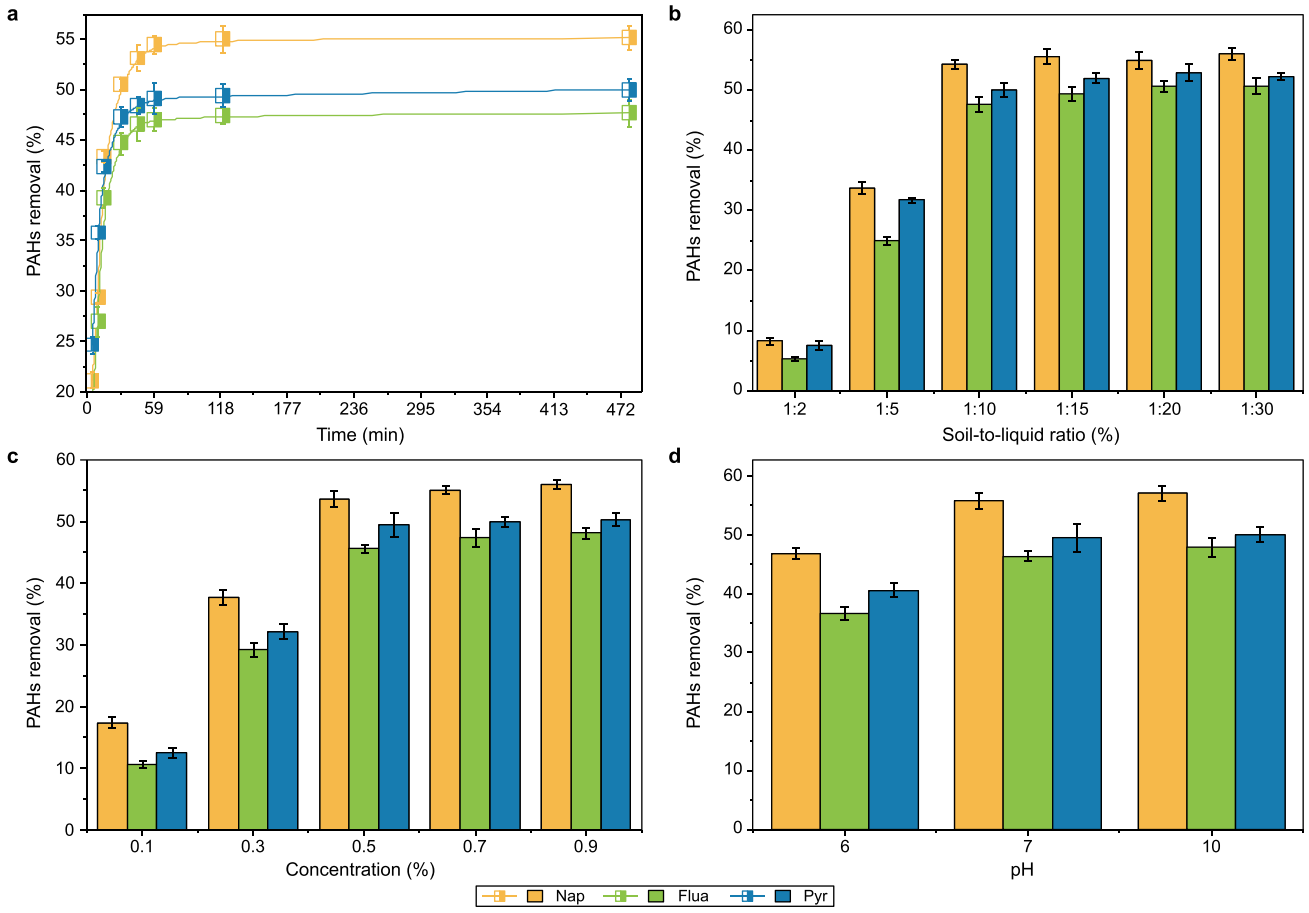


**Fig. 7.** The impact of time (**a**), soil-to-liquid ratio (**b**), concentration (**c**), and pH (**d**) on the desorption efficiency of PAHs.

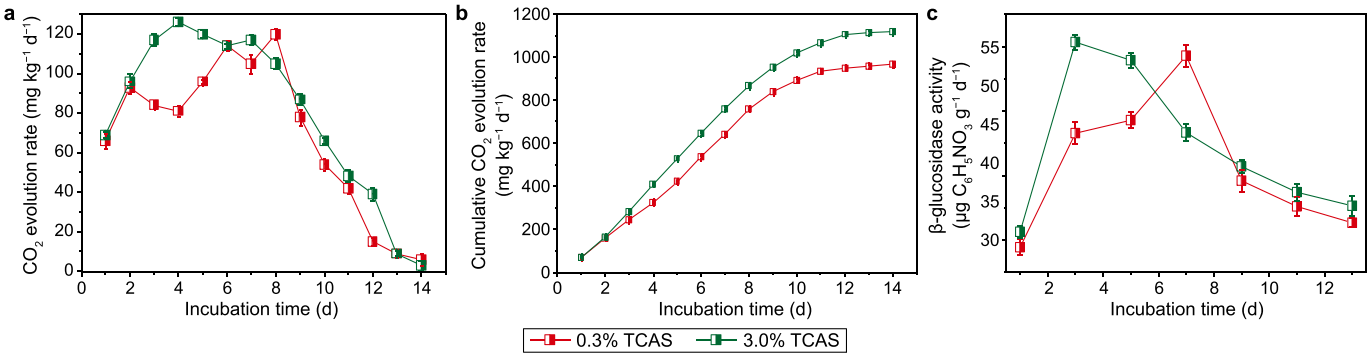


**Fig. 8.** $CO_2$ evolution rate **(a)**, cumulative $CO_2$ emission rate **(b),** and β-glucosidase activity **(c)** response to 0.3% and 3.0% TCAS over 14 days.

PAHs from the TCAS, facilitating desorption. Essentially, a basic pH environment alters the chemical interactions and conformation of TCAS, optimizing it for effective PAH desorption.

### 3.6. Soil quality, enzyme activity, and respiration change

The investigation into TCAS as a soil-washing agent offers promising insights into its application for soil remediation with mindful consideration of its concentration. Fig. 8a indicates that at a lower concentration of 0.3%, TCAS does not severely hinder microbial activity, as evidenced by the $CO_2$ evolution rate, which suggests a stimulated microbial response initially. This stimulation reflects an adaptive microbial activity, possibly due to the utilization of TCAS components or the degradation of existing soil contaminants.

Moreover, the β-glucosidase activity, a key indicator of soil health and microbial function [72], peaks in conjunction with $CO_2$ evolution, further signalling an active, functioning microbial community (Fig. 7c). The enzyme's activity, only moderately diminished at the lower TCAS concentration, indicates a resilience within the soil's microbiota. This resilience suggests that these bacteria can maintain their function despite introducing a remediation agent.

This balance illustrates that TCAS can potentially be optimized to enhance soil decontamination processes while sustaining, or

**Table 2**
Soil quality change before and after soil washing.

| Treatment status | NHs (mg $kg^{-1}$) | HA (mg $kg^{-1}$) | HFs (mg $kg^{-1}$) | TN (g $kg^{-1}$) | TP (g $kg^{-1}$) | TK (g $kg^{-1}$) |
|---|---|---|---|---|---|---|
| Before soil washing | 2.19 ± 0.02 a | 8.74 ± 0.14 a | 2.54 ± 0.10 a | 1.82 ± 0.09 a | 1.14 ± 0.06 a | 17.87 ± 0.06 a |
| 0.3% TCAS washed soil | 1.91 ± 0.11 b | 8.73 ± 0.02 a | 2.25 ± 0.05 b | 1.76 ± 0.08 b | 0.94 ± 0.07 b | 17.73 ± 0.86 b |
| 3.0% TCAS washed soil | 1.82 ± 0.04 c | 8.72 ± 0.09 a | 2.14 ± 0.03 b | 1.61 ± 0.03 c | 0.95 ± 0.04 b | 17.71 ± 0.82 b |

Note: The table presents the measured parameters for unwashed soil and soils washed with 0.3% and 3.0% TCAS. Significant differences ($P < 0.05$) are indicated by distinct letters (a, b, c), following Tukey's HSD post hoc test, with comparisons made within the same soil fraction across different treatments.

even possibly promoting, microbial functions critical to soil health. The maintenance of β-glucosidase activity is particularly notable, as this enzyme plays a vital role in carbon cycling and nutrient availability in soils.

In conclusion, careful calibration of TCAS concentration could harness the agent's soil-washing capabilities without compromising the vitality of the soil microbial ecosystem. This approach underscores a sustainable pathway to soil remediation, offering a silver lining in the quest for environmental restoration strategies that support microbial allies within the soil.

Table 2 shows the nutritional differences before and after washing the soil. The NHs and HFs contents decreased slightly among the four SOM, which may be related to the high molecular weight of SOM and its larger size relative to the TCAS cavity [73]. According to the hard and soft acids and base hypothesis, TCAS can selectively attract soft metal ions because the O and S atoms on the lower bridge are soft bases; nevertheless, this only modestly reduces the total K in the soil. Moreover, significant changes were also not observed in the amounts of N or P.

### 3.7. TCAS adsorption on soil

Soil quality and ecosystems may be permanently harmed if the soil-washing agent is adsorbed on the soil [74]. The effectiveness of TCAS adsorption on clean and spiked soils is shown in Fig. S2. Despite slightly higher TCAS adsorption, even in PAH-contaminated soils, over 90% of the TCAS remained in the soil washing solution, with the remaining TCAS potentially decomposing within 15 d. The TCAS adsorption results supported the insignificant environmental impact of TCA.

## 4. Conclusions

In this study, we synthesized thiacalix[4]arene tetrasulfonate, a novel, highly water-soluble, size-adjustable CAs derivative, as a soil cleaning agent. This study aims to comprehensively examine the desorption efficiency, interaction mechanism, and soil fertility response to TCAS. Both experimental and theoretical analyses indicate that TCAS interacts with PAHs through π-π stacking, OH-π interactions, hydrogen bonding, van der Waals interactions, and electrostatic contact. Compared to the control, the soil underwent minimal nutritional loss after TCAS soil washing, with increased soil respiration and enzyme activity. This study provides a better understanding of the CAs pollutant removal mechanism by analyzing a novel soil-washing agent. However, our primary focus is on the interaction mechanism for a single PAH. Further research is needed on the simultaneous removal of PAHs and heavy metals using TCAS. The insights from this study may benefit future research into TCAS's interactions with other PAHs and pollutants.

## CRediT authorship contribution statement

**Le-Yao Xing:** Conceptualization, Formal Analysis, Writing - Original Draft. **Guan-Han Meng:** Formal Analysis, Visualization, Writing - Original Draft. **Ji-Xian Yang:** Funding Acquisition, Project Administration, Supervision, Writing - Review & Editing. **Ming-Han Xu:** Investigation, Methodology. **Yi-Ming Xu:** Data Curation, Resources. **Hai-Xiao Xie:** Software. **Ai-Jie Wang:** Supervision, Writing - Review & Editing. **Yi-Lu Sun:** Funding Acquisition, Supervision, Writing - Review & Editing.

## Declaration of competing interest

The authors declare that they have no known competing financial interests or personal relationships that could have appeared to influence the work reported in this paper.

## Acknowledgments

The Authors would like to thank the support of the National Key Research and Development Program of China (Grant No. 2019YFC1803804-02) and the Open Project of the Key Laboratory of Environmental Biotechnology, CAS (Grant No. kf2021008).

## Appendix A. Supplementary data

Supplementary data to this article can be found online at https://doi.org/10.1016/j.ese.2024.100422.

## References

[1] J.J. Ortega-Calvo, M.C. Tejeda-Agredano, C. Jimenez-Sanchez, E. Congiu, R. Sungthong, J.L. Niqui-Arroyo, M. Cantos, Is it possible to increase bioavailability but not environmental risk of PAHs in bioremediation, J. Hazard Mater. 261 (2013) 733–745, https://doi.org/10.1016/j.jhazmat.2013.03.042.
[2] Bai, Y., B. Liang, H. Yun, Y. Zhao, Z. Li, M. Qi, X. Ma, C. Huang and A. Wang "Combined bioaugmentation with electro-biostimulation for improved bioremediation of antimicrobial triclocarban and PAHs complexly contaminated sediments."J. Hazard Mater. 403: 123937, https://doi.org/10.1016/j.jhazmat.2020.123937.
[3] S. Kumari, V.D. Rajput, S. Sushkova, T. Minkina, Microbial electrochemical system: an emerging technology for remediation of polycyclic aromatic hydrocarbons from soil and sediments, Environ. Geochem. Health (2022) 1–17, https://doi.org/10.1007/s10653-022-01356-z.
[4] A. Cachada, E. Ferreira da Silva, A.C. Duarte, R. Pereira, Risk assessment of urban soils contamination: the particular case of polycyclic aromatic hydrocarbons, Sci. Total Environ. 551–552 (2016) 271–284, https://doi.org/10.1016/j.scitotenv.2016.02.012.
[5] C. Trellu, E. Mousset, Y. Pechaud, D. Huguenot, E.D. van Hullebusch, G. Esposito, M.A. Oturan, Removal of hydrophobic organic pollutants from soil washing/flushing solutions: a critical review, J. Hazard Mater. 306 (2016) 149–174, https://doi.org/10.1016/j.jhazmat.2015.12.008.
[6] B. Liang, H. Yun, D.Y. Kong, Y.C. Ding, X.K. Li, A.S. Vangnai, A.J. Wang, Bioaugmentation of triclocarban and its dechlorinated congeners contaminated soil with functional degraders and the bacterial community response, Environ. Res. 180 (2020), https://doi.org/10.1016/j.envres.2019.108840.
[7] M. Usman, K. Hanna, S. Haderlein, Fenton oxidation to remediate PAHs in contaminated soils: a critical review of major limitations and counter-strategies, Sci. Total Environ. 569–570 (2016) 179–190, https://doi.org/10.1016/j.scitotenv.2016.06.135.
[8] S. Lanzalaco, S.J. You, V. Conte, Electrochemically Assisted Thermal-Based Technologies for Soil Remediation, Springer International Publishing, 2021, pp. 369–400, https://doi.org/10.1007/978-3-030-68140-1.
[9] S.Č. Alagić, S. Berend, Đ. Veljović, How can plants manage polycyclic aromatic hydrocarbons? May these effects represent a useful tool for effective soil remediation? A review, Clean Technol. Environ. Policy 17 (3) (2015) 597–614, https://doi.org/10.1007/s10098-014-0840-6.
[10] M. Küstner, B. Vodovar, A. Miltner, Fate of 14C-labeled anthracene and hexadecane in compost-manured soil, Appl. Microbiol. Biotechnol. 43 (6) (1995)

1128–1135, https://doi.org/10.1007/BF00166937.
[11] X. Mao, R. Jiang, W. Xiao, Use of surfactants for the remediation of contaminated soils: a review, J. Hazard Mater. 285 (2015) 419–435, https://doi.org/10.1016/BF00166937.
[12] D. Landy, M.H. Pettit, L. Jicsinszky, Remediation technologies using cyclodextrins: an overview, Environ. Chem. Lett. 10 (3) (2012) 225–237, https://doi.org/10.1016/j.jhazmat.2014.12.009.
[13] E.V. Lau, S. Gan, H.K. Ng, Extraction agents for removing polycyclic aromatic hydrocarbons (PAHs) from soil in soil washing technologies, Environ. Pollut. 184 (2014) 640–649, https://doi.org/10.1016/j.envpol.2013.09.010.
[14] E. Da Silva, A. Alves, L. Santos, Biopharmaceutical applications of calixarenes, J. Drug Deliv. Sci. Technol. 14 (1) (2004) 3–20, https://doi.org/10.1016/S1773-2247(04)50001-1.
[15] A. Dawn, P. Das, B.K. Banik, Assessment of the in vitro toxicity of calixarenes and a metal-seamed calixarene: a chemical pathway for clinical application, Supramol. Chem. 31 (7) (2019) 425–431, https://doi.org/10.1080/10610278.2019.1616732.
[16] P.Y. Li, Y. Chen, Y. Liu, Calixarene/pillararene-based supramolecular selective binding and molecular assembly, Chin. Chem. Lett. 30 (6) (2019) 1190–1197, https://doi.org/10.1016/j.jhazmat.2014.10.056.
[17] B. Mokhtari, K. Pourabdollah, N. Dalali, Analytical applications of calixarenes from 2005 up-to-date, J. Inclusion Phenom. Macrocycl. Chem. 69 (1–2) (2011) 1–55, https://doi.org/10.1007/s10847-010-9848-7.
[18] O. Kundrát, V. Eigner, P. Cuřínová, J. Kroupa, P. Lhoták, Anion binding by meta ureido-substituted thiacalix[4]arenes, Tetrahedron 67 (43) (2011) 8367–8372, https://doi.org/10.1016/j.tet.2011.08.062.
[19] M. Yamada, M. Rajiv Gandhi, U.M.R. Kunda, F. Hamada, Thiacalixarenes: emergent supramolecules in crystal engineering and molecular recognition(TCA), J. Inclusion Phenom. Macrocycl. Chem. 85 (1–2) (2016) 1–18, https://doi.org/10.1007/s10847-016-0616-1.
[20] Y. Agrawal, J. Pancholi, Analytical Applications of Thiacalixarenes: A review(TCA), 2007.
[21] D.-S. Guo, Y. Liu, Supramolecular chemistry of p-Sulfonatocalix[n]arenes and its biological applications, Accounts Chem. Res. 47 (7) (2014) 1925–1934, https://doi.org/10.1021/ar500009g.
[22] A.C. Bhasikuttan, J. Mohanty, Detection, inhibition and disintegration of amyloid fibrils: the role of optical probes and macrocyclic receptors, Chem. Commun. 53 (19) (2017) 2789–2809, https://doi.org/10.1039/c6cc08727b.
[23] S. Manzetti, Chemical and electronic properties of polycyclic aromatic hydrocarbons: a review, in: Handbook of Polycyclic Aromatic Hydrocarbons: Chemistry, Occurrence and Health Issues, 423, 2012, p. 435.
[24] N. Kon, N. Iki, Y. Sano, S. Ogawa, C. Kabuto, S. Miyano, Tuning of the cavity of water-soluble thiacalix 4 arene for the control of inclusion ability toward water-miscible organic molecules, Collect. Czech Chem. Commun. 69 (5) (2004) 1080–1096, https://doi.org/10.1135/cccc20041080.
[25] H. Kumagai, M. Hasegawa, S. Miyanari, Y. Sugawa, Y. Sato, T. Hori, S. Ueda, H. Kamiyama, S. Miyano, Facile synthesis of p-tert-butylthiacalix[4]arene by the reaction of p-tert-butylphenol with elemental sulfur in the presence of a base(TCA), Tetrahedron Lett. 38 (22) (1997) 3971–3972, https://doi.org/10.1016/s0040-4039(97)00792-2.
[26] N. Morohashi, N. Iki, A. Sugawara, S. Miyano, Selective oxidation of thiacalix[4]arenes to the sulfinyl and sulfonyl counterparts and their complexation abilities toward metal ions as studied by solvent extraction, Tetrahedron 57 (26) (2001) 5557–5563, https://doi.org/10.1016/S0040-4039(98)01645-1.
[27] R.O. Miller, R. Gavlak, D. Horneck, Soil, Plant and Water Reference Methods for the Western Region, Colorado State University, Fort Collins, CO, USA, 2013, p. 155.
[28] EPA, SW-846 Test Method 9081: Cation-Exchange Capacity of Soils (Sodium Acetate), EPA, 1986.
[29] F.T. Ramos, E.F. G.d.C. Dores, O.L.d.S. Weber, D.C. Beber, J.H. Campelo Jr., J.C.d.S. Maia, Soil organic matter doubles the cation exchange capacity of tropical soil under no-till farming in Brazil, J. Sci. Food Agric. 98 (9) (2018) 3595–3602, https://doi.org/10.1002/jsfa.8881.
[30] Y. Lin, Z. Li, S. Lv, H. Huang, J. Hu, Detection of soil total nitrogen, phosphorus and potassium content based on the spectral information of citrus canopy, Am. J. Biochem. Biotechnol. 16 (2020) 177–183.
[31] A. Ukalska-Jaruga, R. Bejger, G. Debaene, B. Smreczak, Characterization of soil organic matter individual fractions (fulvic acids, humic acids, and humins) by spectroscopic and electrochemical techniques in agricultural soils, Agronomy 11 (6) (2021) 1067, https://doi.org/10.3390/agronomy11061067.
[32] E. Jez, C. Bravo, D. Lestan, S. Gluhar, L. Martin-Neto, M. De Nobili, M. Contin, Changes in organic matter composition caused by EDTA washing of two soils contaminated with toxic metals, Environ. Sci. Pollut. Control Ser. 28 (46) (2021) 65687–65699, https://doi.org/10.1007/s11356-021-15406-z.
[33] U. US EPA, Method 3540C–Soxhlet Extraction, 1996.
[34] Gaussian 09, Revision D.01, M. J. Frisch, G. W. Trucks, H. B. Schlegel, G. E. Scuseria, M. A. Robb, J. R. Cheeseman, G. Scalmani, V. Barone, B. Mennucci, G. A. Petersson, H. Nakatsuji, M. Caricato, X. Li, H. P. Hratchian, A. F. Izmaylov, J. Bloino, G. Zheng, J. L. Sonnenberg, M. Hada, M. Ehara, K. Toyota, R. Fukuda, J. Hasegawa, M. Ishida, T. Nakajima, Y. Honda, O. Kitao, H. Nakai, T. Vreven, J. A. Montgomery, Jr., J. E. Peralta, F. Ogliaro, M. Bearpark, J. J. Heyd, E. Brothers, K. N. Kudin, V. N. Staroverov, T. Keith, R. Kobayashi, J. Normand, K. Raghavachari, A. Rendell, J. C. Burant, S. S. Iyengar, J. Tomasi, M. Cossi, N. Rega, J. M. Millam, M. Klene, J. E. Knox, J. B. Cross, V. Bakken, C. Adamo, J. Jaramillo, R. Gomperts, R. E. Stratmann, O. Yazyev, A. J. Austin, R. Cammi, C. Pomelli, J. W. Ochterski, R. L. Martin, K. Morokuma, V. G. Zakrzewski, G. A. Voth, P. Salvador, J. J. Dannenberg, S. Dapprich, A. D. Daniels, O. Farkas, J. B. Foresman, J. V. Ortiz, J. Cioslowski, and D. J. Fox, Gaussian, Inc., Wallingford CT, 2013.
[35] Y. Zhao, D.G. Truhlar, The M06 suite of density functionals for main group thermochemistry, thermochemical kinetics, noncovalent interactions, excited states, and transition elements: two new functionals and systematic testing of four M06-class functionals and 12 other functionals, Theor. Chem. Acc. 120 (1) (2008) 215–241, https://doi.org/10.1007/s00214-007-0310-x.
[36] Y. Zhao, N.E. Schultz, D.G. Truhlar, Design of density functionals by combining the method of constraint satisfaction with parametrization for thermochemistry, thermochemical kinetics, and noncovalent interactions, J. Chem. Theor. Comput. 2 (2) (2006) 364–382, https://doi.org/10.1021/ct0502763.
[37] J.W. Hehre, L. Random, P.V.R. Scheyes, J.A. Pople, Ab initio molecular orbital theory, J. Comput. Chem. 7 (3) (1986) 379, https://doi.org/10.1002/jcc.540070314, 379.
[38] T. Lu, Q. Chen, Independent gradient model based on Hirshfeld partition: a new method for visual study of interactions in chemical systems, J. Comput. Chem. 43 (8) (2022) 539–555, https://doi.org/10.1002/jcc.26812.
[39] T. Lu, F. Chen, Multiwfn: a multifunctional wavefunction analyzer, J. Comput. Chem. 33 (5) (2012) 580–592. http://onlinelibrary.wiley.com/doi/10.1002/jcc.22885.
[40] D.A. Angers, S. Recous, Decomposition of wheat straw and rye residues as affected by particle size, Plant Soil 189 (2) (1997) 197–203, https://doi.org/10.1023/A:1004207219678.
[41] M. Tabatabai, "Soil enzymes." Methods of soil analysis: Part 2 Microbiological and biochemical properties 5: 775-833. https://doi.org/10.2136/sssabookser5.2.c37, 1994.
[42] S.K. Papageorgiou, E.P. Kouvelos, E.P. Favvas, A.A. Sapalidis, G.E. Romanos, F.K. Katsaros, Metal–carboxylate interactions in metal–alginate complexes studied with FTIR spectroscopy, Carbohydr. Res. 345 (4) (2010) 469–473, https://doi.org/10.1016/j.carres.2009.12.010.
[43] A.B.D. Nandiyanto, R. Oktiani, R. Ragadhita, How to read and interpret FTIR spectroscope of organic material, Indones. J. Sci. Technol. 4 (1) (2019) 97, https://doi.org/10.17509/ijost.v1i2.
[44] E. Maltseva, C.J. Mackie, A. Candian, A. Petrignani, X. Huang, T.J. Lee, A.G.G.M. Tielens, J. Oomens, W.J. Buma, High-resolution IR absorption spectroscopy of polycyclic aromatic hydrocarbons in the 3 μm region: role of hydrogenation and alkylation, Astron. Astrophys. 610 (2018) A65, https://doi.org/10.1051/0004-6361/201935631.
[45] M. Heger, R.A. Mata, M.A. Suhm, Soft hydrogen bonds to alkenes: the methanol–ethene prototype under experimental and theoretical scrutiny, Chem. Sci. 6 (7) (2015) 3738–3745, https://doi.org/10.1039/C5SC01002K.
[46] A.K. Lemmens, D.B. Rap, J.M.M. Thunnissen, B. Willemsen, A.M. Rijs, Polycyclic aromatic hydrocarbon formation chemistry in a plasma jet revealed by IR-UV action spectroscopy, Nat. Commun. 11 (1) (2020) 269, https://doi.org/10.1038/s41467-019-14092-3.
[47] C.F. Holder, R.E. Schaak, Tutorial on Powder X-ray Diffraction for Characterizing Nanoscale Materials:cause noticeable peaks broading because of amorphous), ACS Nano 13 (7) (2019) 7359–7365, https://doi.org/10.1021/acsnano.9b05157.
[48] M. Ma, Y. Guan, C. Zhang, J. Hao, P. Xing, J. Su, S. Li, X. Chu, A. Hao, Stimulus-responsive supramolecular vesicles with effective anticancer activity prepared by cyclodextrin and ftorafur, Colloids Surf. A Physicochem. Eng. Asp. 454 (2014) 38–45, https://doi.org/10.1016/j.colsurfa.2014.04.005.
[49] S.V. Patil, S.P. Gejji, V.S. Kalyani, D.D. Malkhede, Hydroxycoumarin encapsulated sulfonatothiacalix[4]arene: 1H NMR, steady state fluorescence and theory, J. Mol. Liq. 339 (2021) 116760, https://doi.org/10.1016/j.molliq.2021.116760.
[50] S.T. Gawhale, N.V. Rathod, V.S. Kalyani, P.K. Singh, R.S. Sapkal, V.S. Sapkal, G.N. Chaudhari, D.D. Malkhede, Investigation of host-guest complexation of the ternary model: p-Sulfonatothiacalix[4]arene-fluorescein-M2+, Polyhedron 177 (2020) 114268 https://doi.org/10.1016/j.poly.2019.114268.
[51] N. Roy, P. Bomzan, B. Ghosh, M.N. Roy, A combined experimental and theoretical study on p-sulfonatothiacalix 4 arene encapsulated sulisobenzone, New J. Chem. 47 (3) (2023) 1045–1049, https://doi.org/10.1039/D2NJ05291A.
[52] A.B. Jarange, S.V. Patil, D.D. Malkhede, S.M. Deodhar, V.S. Nandre, S.V. Athare, K.M. Kodam, S.P. Gejji, p-Sulfonatocalixarene versus p-thiasulfonatocalixarene: encapsulation of tenofovir disoproxil fumarate and implications to ESI-MS, HPLC, NMR, DFT and anti-MRSA activities, J. Inclusion Phenom. Macrocycl. Chem. 99 (1–2) (2021) 43–59, https://doi.org/10.1007/s10847-020-01022-w.
[53] P. Bomzan, N. Roy, B. Ghosh, M.N. Roy, Exploring inclusion complexes of amino acids with p-sulfonatothiacalix[4]arene by experimental and computational approach, J. Mol. Struct. 1271 (2023) 133981, https://doi.org/10.1515/zpch-2019-1500.
[54] H.L. Hong, J.F. Sun, Y. Zhang, N. Zhu, L.M. Han, Q.L. Suo, Preparation, characterization and in vitro evaluation of tosufloxacin tosylate and hydroxypropyl-beta-cyclodextrin inclusion complex (NMR), Indian J. Pharmaceut. Sci. 81 (2) (2019), https://doi.org/10.36468/pharmaceutical-sciences.505.
[55] P. Michalska, A. Wojnicz, A. Ruiz-Nuno, S. Abril, I. Buendía, R. León, Inclusion complex of ITH12674 with 2-hydroxypropyl-β-cyclodextrin: preparation, physical characterization and pharmacological effect, Carbohydr. Polym. 157 (2017) 94–104, https://doi.org/10.1016/j.carbpol.2016.09.072.
[56] T.D. Claridge, High-resolution NMR Techniques in Organic Chemistry, Elsevier, 2016.

[57] P. Bomzan, N. Roy, B. Ghosh, M.N. Roy, Exploring inclusion complexes of amino acids with p-sulfonatothiacalix[4]arene by experimental and computational approach, J. Mol. Struct. 1271 (2023) 133981, https://doi.org/10.1016/j.molstruc.2022.133981.
[58] N.N. Valand, M.B. Patel, S.K. Menon, Curcumin-p-sulfonatocalix[4]resorcinarene (p-SC[4]R) interaction: thermo-physico chemistry, stability and biological evaluation, RSC Adv. 5 (12) (2015) 8739–8752, https://doi.org/10.1039/c4ra12047gv.
[59] X. Shen, M. Belletête, G. Durocher, Studies of the inclusion complexation between a 3H-indole and β-cyclodextrin in the presence of urea, sodium dodecyl sulfate, and 1-propanol, Langmuir 13 (22) (1997) 5830–5836, https://doi.org/10.1039/C4RA12047G.
[60] M.K. Abd El-Rahman, A.M. Mahmoud, A novel approach for spectrophotometric determination of succinylcholine in pharmaceutical formulation via host–guest complexation with water-soluble p-sulfonatocalixarene, RSC Adv. 5 (77) (2015) 62469–62476, https://doi.org/10.1039/C5RA10166B.
[61] B. Ghosh, N. Roy, S. Mandal, S. Ali, P. Bomzan, D. Roy, M. Salman Haydar, V.K. Dakua, A. Upadhyay, D. Biswas, K.K. Paul, M.N. Roy, Host–guest encapsulation of RIBO with TSC4X: synthesis, characterization, and its application by physicochemical and computational investigations, ACS Omega 8 (7) (2023) 6778–6790, https://doi.org/10.1021/acsomega.2c07396.
[62] N.B. ElDin, M.K. Abd El-Rahman, H.E. Zaazaa, A.A. Moustafa, S.A. Hassan, Supramolecular green chemistry; an eco-friendly spectrophotometric approach for determination of non-chromophoric methacholine via host-guest interactions with 4-sulfocalix[4]arene, Microchem. J. 168 (2021) 106419, https://doi.org/10.1016/j.microc.2021.106419.
[63] H.A. Benesi, J. Hildebrand, A spectrophotometric investigation of the interaction of iodine with aromatic hydrocarbons, J. Am. Chem. Soc. 71 (8) (1949) 2703–2707, https://doi.org/10.1021/ja01176a030.
[64] R. Singh, S. Mahanta, A. Bagchi, N. Guchhait, Interaction of human serum albumin with charge transfer probe ethyl ester of N,N-dimethylamino naphthyl acrylic acid: an extrinsic fluorescence probe for studying protein microenvironment, Photochem. Photobiol. Sci. : Off. J. Eur. Photochem. Assoc. Eur. Soc. Photobiol. 8 (2009) 101–110, https://doi.org/10.1039/b814050b.
[65] A.A. Abdel-Shafi, Spectroscopic studies on the inclusion complex of 2-naphthol-6-sulfonate with β-cyclodextrin, Spectrochim. Acta Mol. Biomol. Spectrosc. 66 (3) (2007) 732–738, https://doi.org/10.1016/j.saa.2006.04.018.
[66] M. Chen, G.W. Diao, Intermolecular complexation between p-sulfonated calix[4,6,8]arene sodium and neutral red, J. Solut. Chem. 40 (3) (2011) 481–491, https://doi.org/10.1007/s10953-011-9660-z.
[67] K. Wang, S.Y. Xing, X.G. Wang, H.X. Dou, The effect of terminal groups of viologens on their binding behaviors and thermodynamics upon complexation with sulfonated calixarenes, Org. Biomol. Chem. 13 (19) (2015) 5432–5443, https://doi.org/10.1039/C5OB00053J.
[68] Y. Liu, D.-S. Guo, H.-Y. Zhang, Y.-H. Ma, E.-C. Yang, The structure and thermodynamics of calix[n]arene complexes with dipyridines and phenanthroline in aqueous solution studied by microcalorimetry and NMR spectroscopy, J. Phys. Chem. B 110 (7) (2006) 3428–3434, https://doi.org/10.1021/jp0545703.
[69] J. Contreras-García, E.R. Johnson, S. Keinan, R. Chaudret, J.-P. Piquemal, D.N. Beratan, W. Yang, NCIPLOT: a program for plotting noncovalent interaction regions, J. Chem. Theor. Comput. 7 (3) (2011) 625–632, https://doi.org/10.1021/ct100641a.
[70] N. Douteau-Guével, A.W. Coleman, J.-P. Morel, N. Morel-Desrosiers, Complexation of the basic amino acids lysine and arginine by three sulfonatocalix[n]arenes (n = 4, 6 and 8) in water: microcalorimetric determination of the Gibbs energies, enthalpies and entropies of complexation, J. Chem. Soc., Perkin Trans. 2 (3) (1999) 629–634, https://doi.org/10.1039/A806855K.
[71] Z. Miskolczy, L. Biczók, Photochromism of a merocyanine dye bound to sulfonatocalixarenes: effect of pH and the size of macrocycle on the kinetics(influence of pH), J. Phys. Chem. B 117 (2) (2013) 648–653, https://doi.org/10.1021/jp310167j.
[72] X.-C. Wang, Q. Lu, Beta-glucosidase activity in paddy soils of the Taihu lake region, China, Pedosphere 16 (1) (2006) 118–124, https://doi.org/10.1016/S1002-0160(06)60033-7.
[73] M. Kleber, M.G. Johnson, Advances in understanding the molecular structure of soil organic matter: implications for interactions in the environment, Adv. Agron. 106 (2010) 77–142, https://doi.org/10.1016/S0065-2113(10)06003-7.
[74] X. Mao, R. Jiang, W. Xiao, J. Yu, Use of surfactants for the remediation of contaminated soils: a review, J. Hazard Mater. 285 (2015) 419–435, https://doi.org/10.1016/j.jhazmat.2014.12.009.